Atmos. Chem. Phys., 5, 493–503, 2005
www.atmos-chem-phys.org/acp/5/493/
SRef-ID: 1680-7324/acp/2005-5-493
European Geosciences Union

Atmospheric Chemistry and Physics

Actinometric measurements of NO_2 photolysis frequencies in the atmosphere simulation chamber SAPHIR

B. Bohn, F. Rohrer, T. Brauers, and A. Wahner

Institut für Chemie und Dynamik der Geosphäre II: Troposphäre, Forschungszentrum Jülich, 52425 Jülich, Germany

Received: 25 October 2004 – Published in Atmos. Chem. Phys. Discuss.: 8 December 2004
Revised: 8 February 2005 – Accepted: 9 February 2005 – Published: 15 February 2005

Abstract. The simulation chamber SAPHIR at Forschungszentrum Jülich has UV permeable teflon walls facilitating atmospheric photochemistry studies under the influence of natural sunlight. Because the internal radiation field is strongly affected by construction elements, we use external, radiometric measurements of spectral actinic flux and a model to calculate mean photolysis frequencies for the chamber volume (Bohn and Zilken, 2005). In this work we determine NO_2 photolysis frequencies $j(NO_2)$ within SAPHIR using chemical actinometry by injecting NO_2 and observing the chemical composition during illumination under various external conditions. In addition to a photo-stationary approach, a time-dependent method was developed to analyse the data. These measurements had two purposes. Firstly, to check the model predictions with respect to diurnal and seasonal variations in the presence of direct sunlight and secondly to obtain an absolute calibration factor for the combined radiometry-model approach. We obtain a linear correlation between calculated and actinometric $j(NO_2)$. A calibration factor of 1.34 ± 0.10 is determined, independent of conditions in good approximation. This factor is in line with expectations and can be rationalised by internal reflections within the chamber. Taking into account the uncertainty of the actinometric $j(NO_2)$, an accuracy of 13% is estimated for the determination of $j(NO_2)$ in SAPHIR. In separate dark experiments a rate constant of $(1.93\pm0.12)\times10^{-14}$ cm^3 s^{-1} was determined for the NO+O_3 reaction at 298 K using analytical and numerical methods of data analysis.

1 Introduction

Photolysis processes are very important for atmospheric chemistry. For example, photolysis of NO_2 followed by reaction of O-atoms with O_2 is a major source of tropospheric ozone:

$$NO_2 + h\nu(\lambda \leq 420\,\text{nm}) \rightarrow O(^3P) + NO \quad (1)$$

$$O(^3P) + O_2 \rightarrow O_3 \quad (2)$$

Photolysis frequencies (j) are first-order rate constants quantifying the rate of photolysis processes in terms of a relative concentration change of the precursor molecule (or a photoproduct). For Reaction (1):

$$j(NO_2) = -\frac{1}{[NO_2]}\frac{d[NO_2]}{dt} \quad (3)$$

Of course, Eq. (3) is valid only in the absence of other NO_2 loss or formation processes and cannot be used to determine $j(NO_2)$ from NO_2 concentration measurements in complex, natural systems. In the troposphere for example, NO_2 loss by photolysis is partly compensated by reaction of NO with O_3 or peroxy radicals (RO_2):

$$NO + O_3 \rightarrow NO_2 + O_2 \quad (4)$$

$$NO + RO_2 \rightarrow NO_2 + RO \quad (5)$$

However, in simpler artificial chemical systems, photolysis frequencies can be determined by monitoring the gas-phase composition. This technique is well established since many years and referred to as chemical actinometry. A recent study by Shetter et al. (2003) gives an overview of previous work concerned with actinometric $j(NO_2)$ measurements. In the case of Reaction (1), a quartz flow-tube exposed to sunlight can be used where the carrier gas is loaded with a known concentration of NO_2. Photolysis frequencies are then determined from the increase of NO concentration as a function of exposure time.

The complex instrumentation needed to obtain a single photolysis frequency is a drawback of chemical actinometry

Correspondence to: B. Bohn
(b.bohn@fz-juelich.de)

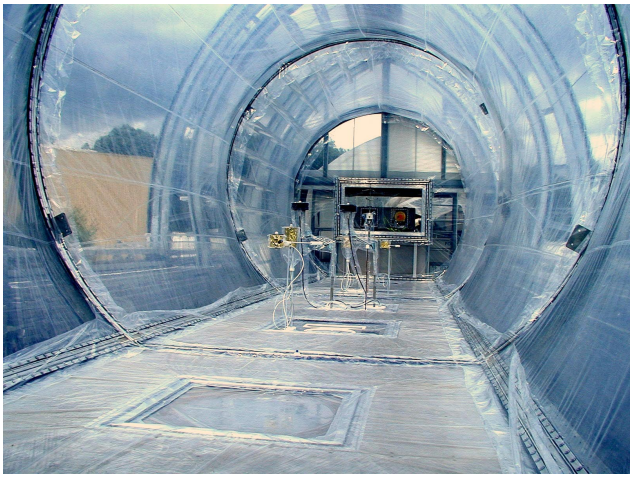

Fig. 1. The atmosphere simulation chamber SAPHIR from inside.

for field measurements. As a consequence, spectroradiometry is a useful alternative where solar spectral actinic flux F_λ is measured and photolysis frequencies are calculated using the absorption cross sections σ of the precursor molecule and the quantum yield ϕ of the photo-products (e.g. Hofzumahaus et al., 1999). In the case of Reaction (1):

$$j(\mathrm{NO_2}) = \int \sigma(\mathrm{NO_2})\,\phi(\mathrm{O^3P})\,F_\lambda(\lambda)\,\mathrm{d}\lambda \qquad (6)$$

Recent comparisons show that chemical actinometry and spectroradiometry give consistent results within better than 10% with respect to NO_2 and O_3 photolyses (Kraus et al., 2000; Shetter et al., 2003; Hofzumahaus et al., 2004). In the case of NO_2 photolysis the agreement is even within 5% in a study from our laboratory (Kraus et al., 2000) using molecular data $\sigma(NO_2)$ and $\phi(O^3P)$ by Merienne et al. (1995) and Troe (2000), respectively, as recently recommended by Atkinson et al. (2004).

The spectroradiometric approach is not as straightforward for the atmosphere simulation chamber SAPHIR at Forschungszentrum Jülich (Fig. 1). SAPHIR was created to study tropospheric chemistry unaffected by transport processes at ambient levels of trace gas concentrations. As in the real troposphere, chemistry is driven by photolysis of trace gases induced by natural sunlight entering the chamber through UV-permeable teflon walls. However, the radiation field inside the chamber is complex and radiometric point measurements are not representative for the reactor as a whole.

In a preceding paper (Bohn and Zilken, 2005) a model was developed predicting time-dependent, volume-mean photolysis frequencies for the simulation chamber. This approach will be denoted SRTM (SAPHIR Radiative Transmission Model) in the following. The model uses external spectroradiometric measurements of direct and diffuse down-welling 2π sr solar actinic flux as input and considers the influence of opaque chamber elements and chamber teflon walls. Basically, time and wavelength dependent, relative scaling factors for the external diffuse and direct fluxes are derived. Time dependent effects are most pronounced for direct sunlight while wavelength dependence is induced by the chamber walls leading to an increase of transmission with wavelength by about 20% in the range 300–400 nm. As an example for the nature and magnitude of the predicted effects, Fig. 2 shows a comparison of $j(NO_2)$ measured externally by a spectroradiometer (SR) and calculated by SRTM. However, so far SRTM calculations are on a relative basis and need confirmation on an absolute level. Moreover, the predicted time-dependencies have to be checked experimentally before this method can be used for routine measurements of photolysis frequencies in SAPHIR, as intended.

In this work we present measurements of $j(NO_2)$ using the simulation chamber as a chemical actinometer. This is achieved by injecting NO_2 into the clean chamber. Upon illumination, photolysis of NO_2 leads to formation of NO and O_3 (Reactions 1 and 2). After a delay dependent on experimental conditions, a photochemical equilibrium establishes where losses of NO_2 by photolysis are compensated by the NO+O_3 reaction. From the equilibrium concentrations of NO, O_3 and NO_2 $j(NO_2)$ can be calculated. In addition we consider deviations from photochemical equilibrium by a time-dependent approach to derive photolysis frequencies under variable external conditions. The actinometric $j(NO_2)$ are then compared with radiometric SRTM predictions. Clear sky conditions at different seasons as well as overcast conditions were investigated. Furthermore, the rate constant of Reaction (4) is determined in separate dark-experiments under the experimental conditions in SAPHIR.

2 Experimental

2.1 Simulation chamber

The simulation chamber SAPHIR consists of a double-wall teflon (FEP) tube held in a steel frame (Fig. 1). FEP film has been selected because it is chemically inert and UV permeable. The inner tube is used as a reactor for simulation experiments. It has a volume of 270 m^3 and can be flushed with dry or wet synthetic air (purity 99.9999%) loaded with a variety of trace gases if required. The space between the inner and the outer tube (≈0.1 m) is permanently flushed with synthetic air to prevent diffusion of gases from outside. Typical leak rates for the reactor are 3–8 m^3 h^{-1}. The chamber can be covered by a movable, opaque roof construction within about 1 min and vice versa. More details concerning the instrumentation and performance of SAPHIR are given by Rohrer et al. (2004).

2.2 Actinometry

In actinometric experiments typically 20–50 ppb of NO_2 (500 ppm in N_2, Messer Griesheim) were injected into the dark chamber filled with dry air in the absence of any VOCs ($\leq$2 ppt, GC analysis). After about 30 min delay to allow for homogeneous mixing, the roof was opened and photochemistry started notable by a decrease of NO_2 concentration and a corresponding increase of NO and O_3 concentrations. Measurements of trace gases were made close to the centre of the chamber 1 m above chamber ground. Ozone was measured by a commercial UV absorption instrument (Ansyco, O3 41M) with a precision of 0.3–0.5 ppb and an accuracy of 3%. NO and NO_2 were measured by a chemiluminescence technique with a modified commercial instrument (Eco Physics, TR 780). The precisions are about 5 ppt and 10 ppt at NO=0 and NO_2=0, respectively, and about 0.1% at 50 ppb for both compounds. NO_2 is photolytically converted to NO prior to detection (Eco Physics, PLC 760). Absolute accuracy and the efficiency of the photolytic converter are checked by regular comparisons with certified NO test gas (2 ppm NO in N_2, BOC Gases) and by gas phase titrations of NO with O_3. The accuracy is 5% for NO, 10% for NO_2 and 5% for the NO/NO_2 ratio. Measurements were made every 50 s with regular switching between NO and NO_2 measurement modes. More details of this technique are given by Rohrer et al. (1998). Temperature and pressure measurements were made using an ultrasonic anemometer (Metek, USA-1) via sound velocity and a capacity pressure gauge (Setra Systems, 270), respectively. Temperature within the reactor cannot be controlled. It typically lies about 0–5 K above ambient temperature, dependent on conditions.

2.3 Spectroradiometry and model calculations

During the actinometric chamber experiments the downwelling 2π sr solar actinic flux was measured externally by a spectroradiometer on the roof of a nearby building. Spectra were recorded about every 2 min in the range 280–420 nm with a distinction of diffuse and direct sunlight by using a shadow ring. More details concerning these measurements are given by Hofzumahaus et al. (1999) and Bohn and Zilken (2005). From these measurements solar actinic flux spectra and photolysis frequencies are derived for the simulation chamber using SRTM calculations (Bohn and Zilken, 2005).

3 Results and discussion

3.1 Rate constant of the O_3+NO reaction

The rate constant of Reaction (4) is essential to determine $j(NO_2)$ by actinometry. k_4 can be obtained in separate dark-experiments by closing the roof of SAPHIR after the actinometric experiments described in Sect. 2.2. NO subsequently reacts with O_3 forming NO_2 until one or both reactants are used up. Although the chemical system is simple, data analysis is not straightforward because starting concentrations of NO and O_3 are not identical. As a consequence, dilution is affecting the reactants differently. Although dilution is slow ($\leq 10^{-5}$ s^{-1}), it cannot be neglected for the dark reactions because the decay of the reactants takes hours at the concentration levels used. On the other hand, dilution can be treated as a first-order loss process for any species because the chamber behaves like an ideal stirred reactor in good approximation.

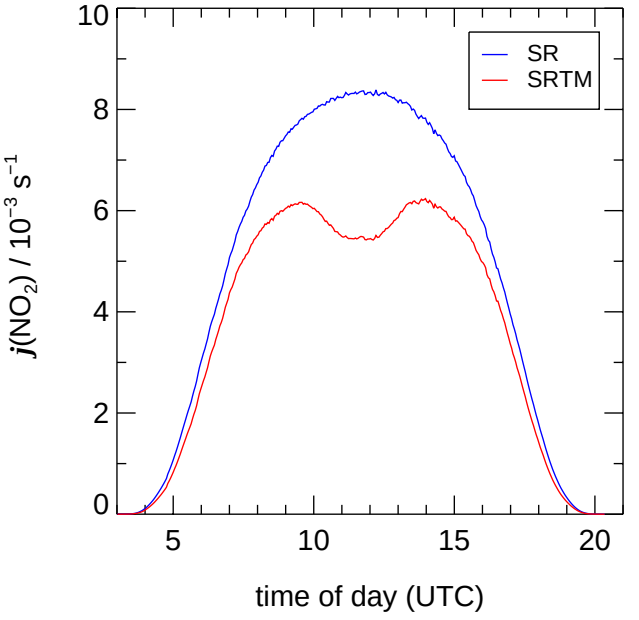

Fig. 2. Diurnal variation of $j(NO_2)$ measured on a clear sky day (28 July 2002) outside the simulation chamber by a spectroradiometer (SR). SRTM predictions for SAPHIR including a preliminary calibration factor of 1.3 (Bohn and Zilken, 2005) are shown for comparison.

The reason for the different starting concentrations of NO and O_3 is the presence of small amounts of HONO produced by the chamber walls at illumination (Rohrer et al., 2004). The formation rate of HONO is usually small at dry conditions ($\approx$50 ppt h^{-1}) but photolysis of HONO leads to a small net production of NO. On the other hand, after a longer period of illumination there is a tendency towards a net O_3 production, probably induced by reaction of OH (from HONO photolysis) with traces of VOCs not accounted for by GC analysis. The background reactivity with respect to OH can be expressed in terms of a hypothetical CO concentration of typically 100–300 ppb (Rohrer et al., 2004). However, CO is just a proxy for unknown reactants because CO levels are continuously monitored and usually below the detection limit (10 ppb). These interferences are leading to certain levels of HO_2 or RO_2 radicals upon illumination (see Sect. 3.2) and small differences of NO and O_3 starting concentrations for the dark experiments.

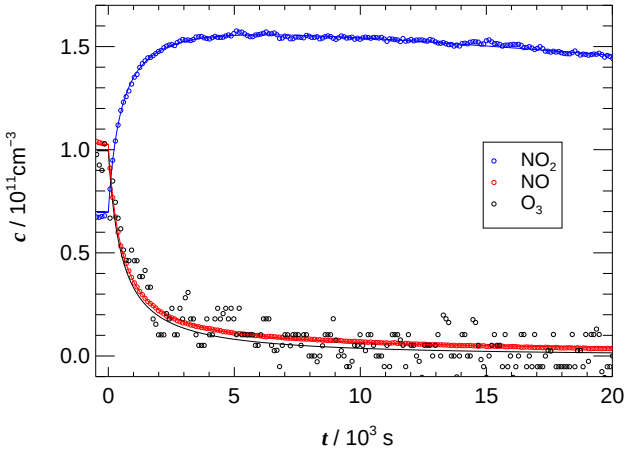

Fig. 3. Concentration traces of NO_2, NO and O_3 after closing the roof of SAPHIR at t=0. Blue, red, and black lines, respectively, show fits from analytical data analysis using NO and NO_2 data.

In the succeeding two sections, analytical and numerical methods of data analysis will be used to determine k_4 from the experimental NO, NO_2 and O_3 concentration traces.

3.1.1 Analytical solution

The dark-reactions can be described by the following set of differential equations:

$$\frac{\mathrm{d[NO]}}{\mathrm{d}t} = -k_4[\mathrm{NO}][\mathrm{O_3}] - k_{\mathrm{dil}}[\mathrm{NO}] \quad (7)$$

$$\frac{\mathrm{d[O_3]}}{\mathrm{d}t} = -k_4[\mathrm{NO}][\mathrm{O_3}] - k_{\mathrm{dil}}[\mathrm{O_3}] \quad (8)$$

$$\frac{\mathrm{d[NO_2]}}{\mathrm{d}t} = k_4[\mathrm{NO}][\mathrm{O_3}] - k_{\mathrm{dil}}[\mathrm{NO_2}] \quad (9)$$

Here k_{dil} is the first-order rate constant of loss by dilution. Utilising the additional relations:

$$[\mathrm{NO_x}] = [\mathrm{NO_2}] + [\mathrm{NO}] = ([\mathrm{NO_2}]_0 + [\mathrm{NO}]_0)\exp(-k_{\mathrm{dil}}\,t) \quad (10)$$

$$[\mathrm{NO}] - [\mathrm{O_3}] = ([\mathrm{NO}]_0 - [\mathrm{O_3}]_0)\exp(-k_{\mathrm{dil}}\,t) \quad (11)$$

the system of differential equations can be reduced to a single equation:

$$\frac{\mathrm{d[NO]}}{\mathrm{d}t} = -k_4[\mathrm{NO}]\{[\mathrm{NO}] - ([\mathrm{NO}]_0 - [\mathrm{O_3}]_0)\exp(-k_{\mathrm{dil}}\,t)\} - k_{\mathrm{dil}}[\mathrm{NO}] \quad (12)$$

This equation was solved using the solution of Bernoulli's differential equation:

$$[\mathrm{NO}] = \frac{D\,([\mathrm{NO}]_0 - [\mathrm{O_3}]_0)}{1 - [\mathrm{O_3}]_0/[\mathrm{NO}]_0\exp\{k_4/k_{\mathrm{dil}}\,([\mathrm{NO}]_0 - [\mathrm{O_3}]_0)\,(D-1)\}} \quad (13)$$

Table 1. Approximate NO and NO_2 starting concentrations ($[O_3]_0 \approx [NO]_0$), experiment durations, temperatures, and fitted scaling factors f_4 (Eq. 14) from four dark-experiments investigating Reaction (4). Scaling factors using analytical and numerical data analysis are given.

$[NO]_0$[a]	$[NO_2]_0$[a]	time/h	T/K[b]	f_4[c]	f_4[d]
1.1	0.7	6	295	1.017	–[e]
3.0	5.0	3	293	1.009	0.956
1.1	0.5	6	295	1.028	1.022
0.4	0.3	6	298	1.003	0.986
			average	1.014±0.014	0.988±0.034

[a] Units are 10^{11} cm^{-3}, [b] mean temperature at early stage of experiments (see text), [c] analytical result, [d] numerical result, [e] no flow rate measurements available.

where $D = \exp(-k_{\mathrm{dil}}\,t)$. From this solution, NO_2 and O_3 concentrations can be calculated by inserting into Eqs. (10) and (11).

Figure 3 shows an example of NO, NO_2 and O_3 concentration traces after closing the roof of SAPHIR. In the data analysis Eqs. (13) and (10) were fitted simultaneously to NO and NO_2 data, respectively, using a Levenberg-Marquardt least-squares fitting procedure. O_3 data were not used because of their poorer precision. Five parameters were determined: the starting concentrations $[NO]_0$, $[NO_2]_0$ and $[O_3]_0$ and the rate constants k_{dil} and k_4.

In Table 1 conditions of four experiments are summarised. Temperatures could not be kept constant and typically decreased by 6–8 K during the experiments. The temperatures listed in Table 1 are averages from the early periods of the experiments in which the NO concentrations dropped to 10% of the starting concentrations (within about 1–2 h after closing the roof). These temperatures are accurate within about 1 K and were assigned to the rate constants obtained from the fits. However, the temperatures of Table 1 are not representative for the later periods of the experiments where temperatures dropped more strongly. The numerical analysis described in the next section therefore uses actual temperatures for the whole period and rate constants k_4 are determined in terms of scaling factors with respect to a currently recommended temperature dependent rate expression (Sander et al., 2003):

$$f_4 = \frac{k_4(T)}{3.0\times10^{-12}\mathrm{cm^3 s^{-1}}\exp(-1500\mathrm{K}/T)} \quad (14)$$

To allow a comparison these scaling factors are also used here to specify the analytical results listed in Table 1.

In all four experiments the scaling factors are close to unity within 3%. The average corresponds to a rate constant of 1.98×10^{-14} cm^3 s^{-1} at 298 K. A 5% error is estimated for the assumption of constant temperatures during the experiments. Together with the uncertainties of the NO_x measurements we evaluate a 7% error limit for the rate constant. To

check for consistency, dilution rate constants were also determined by fitting the exponential decay D of Eq. (13) to the NO_x data. The k_{dil} are similar within 2% compared to the results obtained by fitting Eq. (13).

3.1.2 Numerical analysis

Equation (13) shows that analytical solutions are getting complex and inflexible even for a fairly simple chemical system. A drawback of Eq. (13) is that dilution and temperature are assumed constant during the experiments. Although this is correct in good approximation, the use of measured, time-dependent temperatures and dilution rates calculated from the flow rates of the gas-supplying system (Rohrer et al., 2004) are more appropriate. For that reason a numerical method was used where time-dependent experimental boundary conditions are considered and the system of differential equations (Eqs. 7–9) is solved numerically using EASY (Brauers and Rohrer, 1999) which is an interface for the FACSIMILE integrator with time dependent boundary values and the Levenberg-Marquardt algorithm for fitting. The results of the numerical data analysis are also summarised in Table 1. Only three experiments could be analysed because flow rates were not monitored in one of the experiments. The averaged scaling factor corresponds to a rate constant of 1.93×10^{-14} cm^3 s^{-1} at 298 K. Taking into account the uncertainty of the NO_x measurements and the reproducibility of the result, we estimate a 6% error limit for this rate constant.

In the numerical approach also the slow reaction:

$$NO_2 + O_3 \rightarrow NO_3 + O_2 \quad (15)$$

and consecutive reactions of the NO_3 radical were considered, e.g. the fast reaction NO_3+NO$\rightarrow$2 NO_2. However, switching off Reaction (15) in the numerical analysis led to fitted scaling factors within 1% compared to the full model, i.e. neglecting Reaction (15) in the analytical approach is justified.

In summary, both methods of data analysis yield consistent results with averaged scaling factors very close to unity within 2%. Our data therefore confirm the recommendation by Sander et al. (2003) (Eq. 14, k_4(298 K)=1.95×10^{-14} cm^3 s^{-1}) which will be used in the following experiments aiming at photolysis frequencies. It should be noted that a recently recommended Arrhenius expressions by Atkinson et al. (2004) is lower by 12% at 298 K.

3.2 Photolysis frequencies from trace gas concentrations

The idea behind chamber actinometry is to derive mean photolysis frequencies from concentrations of trace gases within the reactor. After injection of NO_2 into the chamber, photolysis of NO_2 leads to formation of O_3 and NO. On the other hand, reaction of these photo-products regenerates NO_2. A

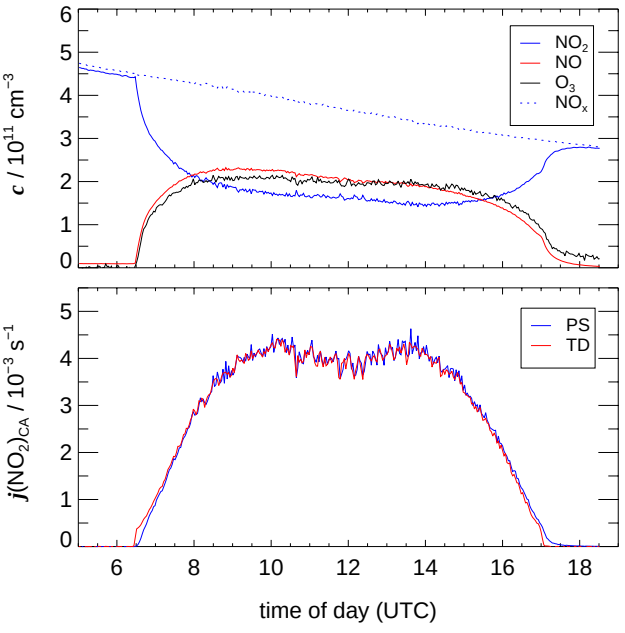

Fig. 4. Upper panel: concentration traces of NO_2, NO and O_3 in an actinometric experiment on 10 March 2002 under clear sky conditions. Lower panel: actinometric photolysis frequencies calculated using the photo-stationary (PS) and the time-dependent (TD) approach.

photochemical equilibrium has established if loss and formation processes compensate each other, e.g. in the case of NO_2:

$$\frac{d[NO_2]}{dt} = -j(NO_2)[NO_2] + k_4[O_3][NO] = 0 \quad (16)$$

Since k_4 is known, $j(NO_2)$ can be calculated from the equilibrium concentrations of NO_2, O_3 and NO:

$$j(NO_2)_{PS} = \frac{k_4[O_3][NO]}{[NO_2]} \quad (17)$$

In this photo-stationary (PS) approach losses by dilution are neglected and $j(NO_2)$ is assumed constant. Dilution is indeed too slow to influence the photochemical equilibrium with $j(NO_2)$ typically more than two orders of magnitude greater than k_{dil}.

The PS approach remains reasonable if $j(NO_2)$ changes slowly compared to the relaxation time of the photochemical system. This is the case for example under clear-sky conditions where $j(NO_2)$ exhibits a smooth change in the course of a day. However, under cloudy conditions $j(NO_2)$ often changes rapidly which leads to a departure from photochemical equilibrium. As a consequence, a different, time-dependent approach (TD) was used to retrieve $j(NO_2)$ from the trace gas concentrations and their changes. The differential equation describing the time-dependence of the NO concentration,

$$\frac{d[NO]}{dt} = -k_4[NO][O_3] + j(NO_2)_{TD}[NO_2] \quad (18)$$

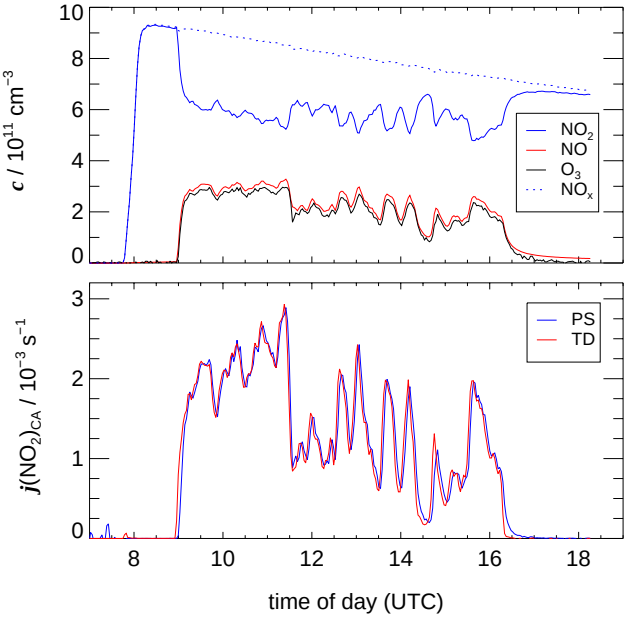

Fig. 5. Upper panel: concentration traces of NO_2, NO and O_3 in an actinometric experiment on 9 March 2002 under overcast conditions. Lower panel: actinometric photolysis frequencies calculated using the photo-stationary (PS) and the time-dependent (TD) approach.

can be rearranged accordingly:

$$j(\mathrm{NO_2})_{\mathrm{TD}} = j(\mathrm{NO_2})_{\mathrm{PS}} + \frac{1}{[\mathrm{NO_2}]}\frac{\mathrm{d}\,[\mathrm{NO}]}{\mathrm{d}\,t} \approx j(\mathrm{NO_2})_{\mathrm{PS}} + \frac{1}{[\mathrm{NO_2}]}\frac{\Delta\,[\mathrm{NO}]}{\Delta\,t} \quad (19)$$

As an example Fig. 4 shows the variation of trace gas concentrations in a typical actinometric experiment on a clear sky day (10 March 2002). After a short delay upon opening the roof, a photochemical equilibrium establishes and concentrations change smoothly in the course of the day. Accordingly, also the actinometric photolysis frequencies $j(\mathrm{NO_2})_{\mathrm{CA}}$ show a smooth change with a local minimum at noon caused by chamber construction elements. Except from short periods directly after opening and closing the roof of SAPHIR, the $j(\mathrm{NO_2})_{\mathrm{CA}}$ based on photo-stationary (PS) and time-dependent (TD) calculations look very similar.

The concentration changes in Fig. 4 are superposed by continuous dilution as reproduced by NO_x. Although the experiment starts with a small residue of NO left behind from an actinometric experiment on the previous day (Fig. 5), there is a slight built-up of O_3 resulting in a residue of about 1 ppb at the end of the day. These imbalances were explained qualitatively in Sect. 3.1. However, the influence of the underlying processes on the photochemical equilibrium are insignificant. For example, if a formation rate of 1 ppb/h of O_3 is assumed as an upper limit and attributed to NO_2 photolysis preceded by oxidation of NO by HO_2 (or RO_2) radicals, the

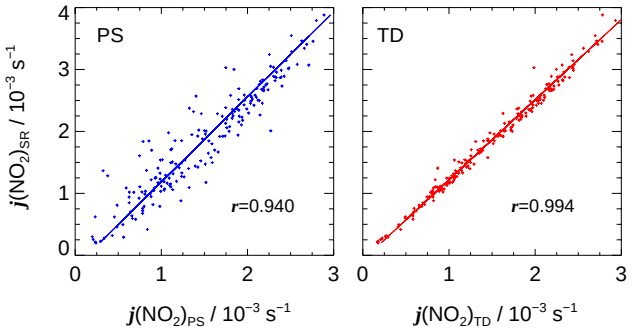

Fig. 6. Correlations of $j(\mathrm{NO_2})_{\mathrm{SR}}$ measured externally with a spectroradiometer and inside SAPHIR by actinometry on an overcast day (9 March 2002). Left: photo-stationary calculation (PS), right: time-dependent approach (TD). Linear correlation coefficients r are indicated.

contribution to the continuous, total NO_2 formation (mainly by NO+O_3) is well below 1%.

Figure 5 shows an experiment on an overcast day (9 March 2002) where occasionally photolysis frequencies changed rapidly. This results in strong changes of trace gas concentrations and sporadic deviations from photochemical equilibrium as indicated by the differences of actinometric PS and TD photolysis frequencies. The PS data clearly show a delayed response to the concentration changes. The difference between the data sets is more obvious in Fig. 6 where the $j(\mathrm{NO_2})_{\mathrm{CA}}$ are plotted against radiometric photolysis frequencies $j(\mathrm{NO_2})_{\mathrm{SR}}$ measured outside of SAPHIR by the spectroradiometer. Under overcast conditions there is a linear correlation between the data (Sect. 4). However, the quality of the correlation improves significantly using the time-dependent calculations rather than the photo-stationary approach, as reflected in the correlation coefficients. In the following we will use the time-dependent approach for all types of conditions, i.e. $j(\mathrm{NO_2})_{\mathrm{CA}}$=$j(\mathrm{NO_2})_{\mathrm{TD}}$.

4 Comparison of actinometry with SRTM predictions

4.1 Overcast conditions

If a constant sky radiance distribution is assumed under overcast conditions, a linear correlation between photolysis frequencies measured externally by radiometry and internally by actinometry is expected. Figure 7 shows a plot of external $j(\mathrm{NO_2})_{\mathrm{SR}}$ against $j(\mathrm{NO_2})_{\mathrm{CA}}$ for three overcast days. The correlation of the data is excellent with a linear correlation coefficient of 0.995. The mean ratio $j(\mathrm{NO_2})_{\mathrm{CA}}/j(\mathrm{NO_2})_{\mathrm{SR}}$ is 0.80±0.05, i.e. the radiometric data have to be scaled down by this factor to obtain mean chamber values. A mean ratio is used here rather than a linear regression to give equal weight to all data points irrespective of the $j(\mathrm{NO_2})$ values. The procedure is justified because deviations from the mean

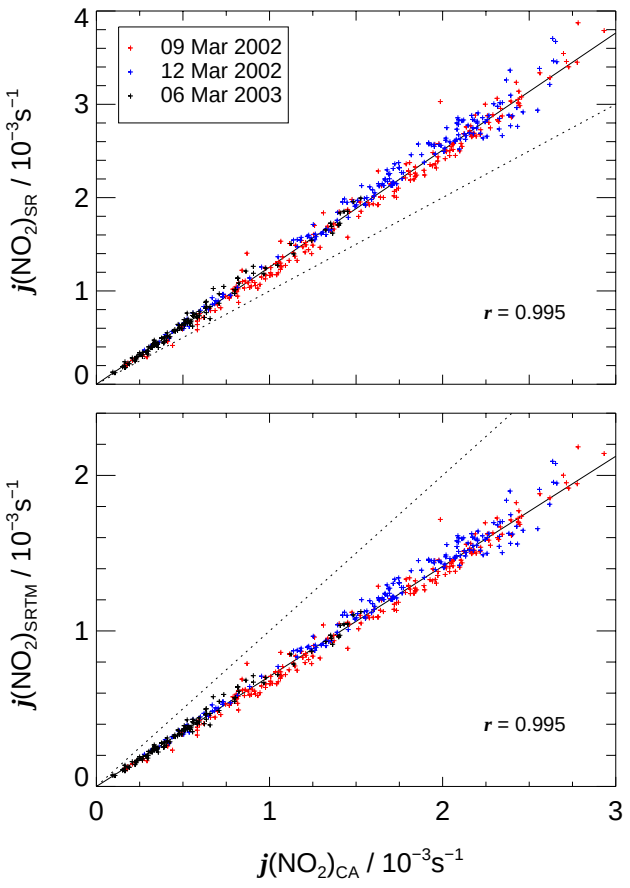

Fig. 7. Upper panel: Correlations of $j(NO_2)_{SR}$ measured externally with a spectroradiometer and $j(NO_2)_{CA}$ from actinometry inside of SAPHIR on three overcast days. Lower panel: Similar plot with radiometric data modified by SRTM calculations. Dotted lines show 1:1 relationships. Linear correlation coefficients r are indicated.

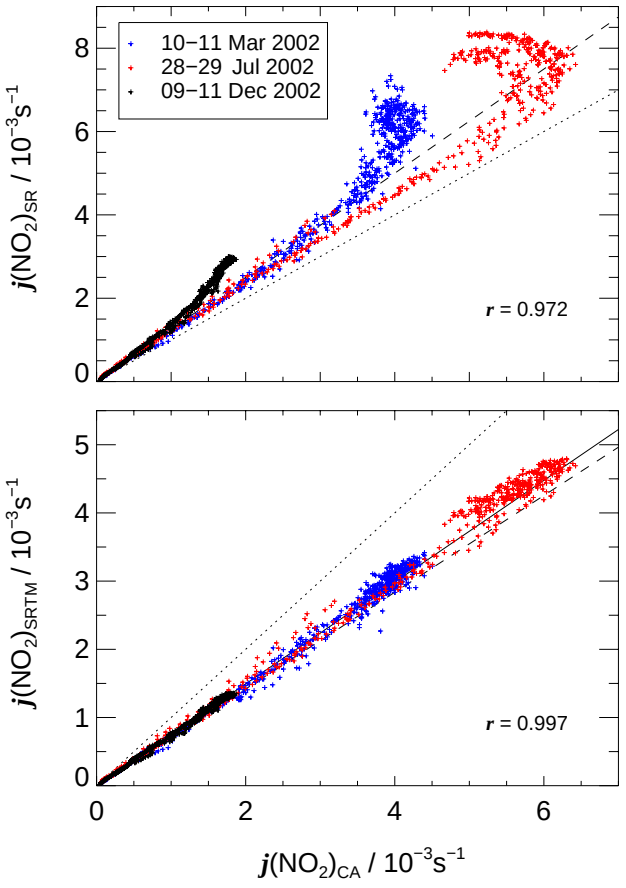

Fig. 8. Upper panel: Correlations of $j(NO_2)_{SR}$ measured externally with a spectroradiometer and $j(NO_2)_{CA}$ from actinometry inside of SAPHIR at a total of seven clear sky days. Different seasons are indicated by colors: black (winter), blue (spring) and red (summer). Lower panel: Similar plot with radiometric data modified by SRTM calculations assuming a UV-A radiance distribution from literature. Dotted lines show 1:1 relationships, dashed lines the results obtained for overcast conditions. Linear correlation coefficients r are indicated.

ratio are normally-distributed in good approximation with a standard deviation stated above.

Of course, also SRTM predicts a linear relationship between $j(NO_2)_{CA}$ and $j(NO_2)_{SR}$. Based on a time-independent SOC sky radiance distribution (standard overcast sky, Grant and Heisler, 1997), scaling factors are calculated theoretically with very minor time-dependent variations introduced by wavelength correction. Accordingly, the plot of $j(NO_2)_{SRTM}$ against $j(NO_2)_{CA}$ in the lower panel of Fig. 7 looks virtually identical and a similar correlation coefficient is obtained. However, the scaling factor necessary to convert SRTM to mean SAPHIR values is different: 1.41±0.09. In contrast to the data measured externally, the model data have to be scaled up because the SRTM calculations are merely dealing with attenuation of radiation by the opaque chamber construction and the limited transmission of the chamber walls. The scaling factor corresponds to the chamber specific quantity $h^c>1$ introduced in SRTM which is rationalised by internal reflections within SAPHIR (Bohn and Zilken, 2005). The effective $h^c_{jNO_2}$ obtained here:

$$h^c_{jNO_2} = \frac{j(NO_2)_{CA}}{j(NO_2)_{SRTM}} \quad (20)$$

is close to an estimate $h^c \approx 1.3$, independent of wavelength, based on 4π radiometric measurements inside the chamber (Bohn and Zilken, 2005). The difference can be explained by an underestimation of chamber wall transmission in the theoretical model. The results of the data analysis for overcast conditions are summarised in Table 2.

The SOC radiance distribution used for the model calculations is an empirical expression with a cosine dependence of radiance on zenith angle (Grant and Heisler, 1997). The applied distribution is about 40% brighter at the zenith and 40% darker at the horizon compared to an isotropic distribution (uniform overcast sky, UOC). However, Bohn and Zilken

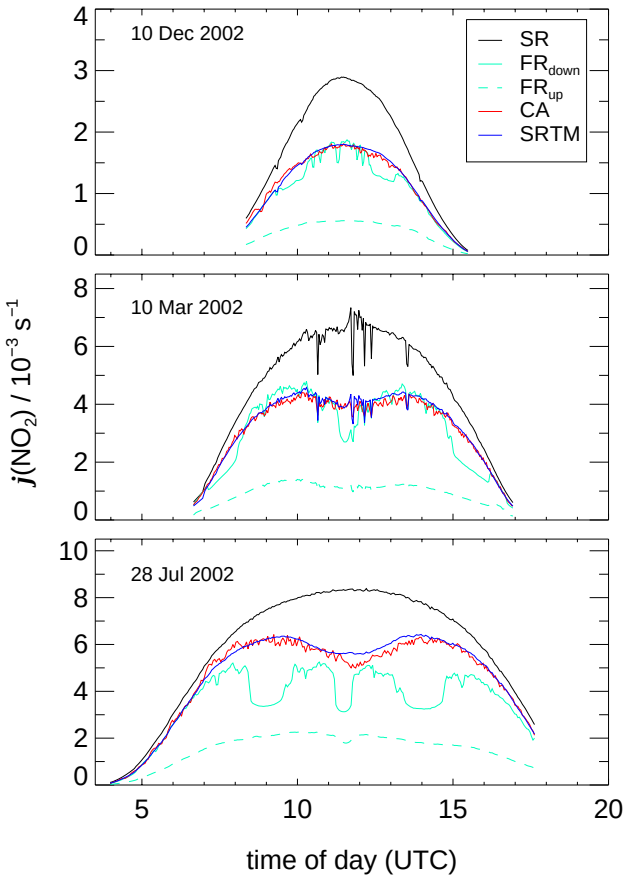

Fig. 9. Examples of diurnal variations of $j(NO_2)$ on the three days of different seasons under clear sky conditions. The external SR data (black) show momentary influence of clouds on 10 March 2002. FR data (green) show local measurements of (up- and downwelling) $j(NO_2)$ inside the chamber using a filterradiometer (see text). SRTM data (blue) were scaled by a factor $h^c_{jNO_2}$=1.34 to fit the CA data (red). Data sets start and end at times where the roof of SAPHIR was opened and closed, respectively.

(2005) show that despite this difference, SOC and UOC radiance distributions give very similar SRTM model results.

4.2 Clear sky conditions

Under clear sky conditions the SRTM model is predicting strong time-dependent chamber effects. In accordance with this, the upper panel of Fig. 8 shows a much poorer correlation between external $j(NO_2)_{SR}$ and internal $j(NO_2)_{CA}$ for a total of seven clear sky days of different seasons. Application of the SRTM model significantly improves this correlation by removing most of the diurnal and seasonal deviations as shown in the lower panel of Fig. 8. The mean ratio $j(NO_2)_{CA}/j(NO_2)_{SRTM}$ yields $h^c_{jNO_2}$=1.34±0.08. Table 2 gives a summary of results for different seasons. Within experimental scatter, there is no seasonal dependence of scaling factors recognisable. Moreover, although the agreement is not perfect, within error limits the $h^c_{jNO_2}$ is similar for overcast conditions.

The SRTM calculations of Fig. 8 are based on an empirical, analytical distribution of diffuse UV-A sky radiance under clear sky conditions (Grant et al., 1997). This is considered the best attempt if no information on radiance distributions is available. However, the quality of the correlation and the factor $h^c_{jNO_2}$ hardly change if the time-independent SOC radiance distribution is used also for clear sky conditions. The reason for this are compensating effects concerning the shadow ring correction and the scaling factors for diffuse sky radiation (Bohn and Zilken, 2005). Using the SOC radiance distribution also for clear sky conditions has two practical benefits. Firstly, less time is needed for the model calculations because a large fraction of computing time is concerned with time-dependent shadow ring corrections and scaling factors of diffuse sky radiation. Secondly, no distinction has to be made within the model between clear sky and overcast conditions.

The effect of neglecting the influence of the chamber walls in the model calculations was also investigated. Bohn and Zilken (2005) already showed that the chamber walls are expected to induce minor time-dependent effects. The largest influence was predicted for direct sunlight during the winter season when the contribution of direct sunlight is low. In accordance with this, the quality of the CA versus SRTM correlations are still satisfactory if the influence of the chamber walls is neglected (r=0.996). On the other hand, the factor $h^c_{jNO_2}$ is lower and close to unity (1.03±0.07) showing that the limited transmission of the chamber walls is almost compensated by internal reflections. However, the $h^c_{jNO_2}$ obtained by neglecting chamber walls in the SRTM calculations cannot be assigned to other photolysis frequencies because no wavelength dependence is considered. Therefore SRTM calculations including chamber walls are preferred.

Taking clear sky and overcast data together and assuming an SOC radiance distribution, we obtain a mean scaling factor $h^c_{jNO_2}$=1.34±0.10 for all conditions, i.e. by the use of external spectroradiometric measurements and the SRTM model we are currently able to determine photolysis frequencies for the simulation chamber within 7–8% of the actinometric reference.

4.3 Limitations and possible error sources

As an example of the remaining differences between actinometric and SRTM data, Fig. 9 shows diurnal variations of photolysis frequencies on three clear sky days of different seasons. Spectroradiometric photolysis frequencies measured outside exhibit a familiar, smooth shape with typical diurnal and seasonal variations. Local measurements of $j(NO_2)$ inside the chamber using a filterradiometer (FR) are strongly influenced by shadows cast by construction elements. Filterradiometers measure integrated actinic flux in a selected wavelength range imitating the relative spectral

Table 2. Linear correlation coefficients r and chamber scaling factors $h^{c}_{jNO_2}$ from a comparison of SRTM and actinometric $j(NO_2)$ data for overcast and clear sky conditions assuming different sky radiance distributions (see text). Error bars correspond to 1σ standard deviations. The results using model inputs considered most realistic are given in bold font.

radiance distribution		UV-A		SOC	
	data points	r	$h^{c}_{jNO_2}$	r	$h^{c}_{jNO_2}$
overcast conditions					
9 March 2002	196		–	0.994	1.44±0.09
12 March 2002	170		–	0.991	1.38±0.06
6 March 2003	118		–	0.995	1.41±0.09
all data	484		–	**0.995**	**1.41±0.09**
clear sky conditions					
9–11 Dec. 2002	481	0.997	1.35±0.08	0.997	1.30±0.09
10–11 March 2002	542	0.994	1.35±0.08	0.993	1.33±0.09
28–29 July 2002	514	0.996	1.31±0.07	0.995	1.31±0.08
all data	1537	**0.997**	**1.34±0.08**	0.996	1.31±0.09
all conditions					
all data	2021		–	0.997	1.34±0.10

response of NO_2 photodissociation (Volz-Thomas et al., 1996). FR calibrations are made by comparisons with the spectroradiometer under field conditions. The FR measurement location was close to the centre of the chamber, 1 m above ground covering both hemispheres separately. The data shown in Fig. 9 confirm that local measurements are inadequate to monitor photolysis frequencies for the simulation chamber under conditions with direct sunlight. On the other hand, actinometric $j(NO_2)$ data and SRTM predictions agree well within experimental scatter. However, the precision of the actinometric data is poorer, limited mainly by the ozone measurements. This induces part of the uncertainties of the $h^{c}_{jNO_2}$. Other possible error sources of more systematic nature which will be discussed in the following.

Taking the actinometric $j(NO_2)$ representative for the chamber volume, assumes well mixed conditions because the radiation field within the chamber is heterogeneous as indicated by the FR measurements. Mixing properties of the chamber were investigated for different conditions. With opened roof there is convection resulting in complete mixing of an injected trace gas pulse within about 10 min. In the dark this mixing time is prolonged by a factor of about three. Operation of two mixing fans shortens the mixing time by a factor of about four. Switching on and off the mixing fans produced no significant change of the measured trace gas concentrations in an actinometric experiment under clear sky conditions where local shadowing should be most pronounced. This shows that mixing within SAPHIR is fast enough to prevent formation of concentration gradients caused by heterogeneous illumination, at least for the photochemical system studied in this work. Nevertheless, small-scale mixing effects can reduce the precision of the actinometric measurements.

Changes of temperature were not considered in the SRTM calculations where T=298 K was assumed. Using a linear interpolation of recommended, temperature dependent data of absorption cross sections and quantum yields of NO_2 (Atkinson et al., 2004), a temperature coefficient of about 0.08% K^{-1} for $j(NO_2)$ is estimated. This has a negligible effect (<1%) on the $h^{c}_{jNO_2}$ scaling factors listed in Table 2.

There seems to be a slight underestimation of the actinometric data by the model calculations in the morning. Such an effect can be explained by different degrees of staining of the chamber foil exposed to atmospheric conditions. Staining can also explain the differences in the scaling factors $h^{c}_{jNO_2}$ obtained for overcast and clear sky conditions. Model calculations seem to over-predict chamber values when direct sunlight is incident from southerly directions passing the upper, more horizontal parts of the chamber walls predestined for staining. However, such effects are hard to assess quantitatively within the model.

With respect to the model, the assumption of a constant SOC sky radiance distribution under overcast conditions is certainly not always matched by reality. Azimuthal variations of sky radiance can produce changes in the actinometric $j(NO_2)$ not noticed by the external radiometric measurement. Under clear sky conditions changes of aerosol load will produce variations in sky radiance distributions. Thus,

the model input can be improved by a measurement of sky radiance distributions as indicated by Bohn and Zilken (2005).

The SRTM model postulates an effective internal amplification of radiation, considered quantitatively by the factor h^c. This amplification is assumed independent of direction of incidence. Moreover, scattering processes at the chamber walls are not explicitly included in the model approach. Both deficiencies can lead to additional time-dependent effects. It is therefore not surprising that model predictions of photolysis frequencies for single locations within the chamber are not well reproduced by measurements. Although the exact time and durations of shadows cast on a location can be predicted, the quantitative effect of these shadows cannot be reproduced. Qualitatively, the light level is higher than predicted in the shadows and lower outside the shadows which can be explained by scattering of radiation at the chamber walls.

Generally also a wavelength dependence of the factor h^c is expected. On the other hand, part of this dependence could already be included in the relative wavelength dependence applied within the SRTM model which is based on a comparison of spectral actinic flux measurements inside and outside the chamber (Bohn and Zilken, 2005). Moreover, 4π measurements within the chamber give no indication for a strong wavelength dependence. For the time being we therefore assume h^c=$h^c_{jNO_2}$ for all wavelengths.

For the accuracy of the $j(NO_2)$ determination within SAPHIR possible systematic errors of the actinometric reference have to be considered as well. Because the uncertainty of the rate constant k_4 is dominated by the uncertainty of the NO_x measurements these errors are not independent and add to 10% for the photolysis frequencies. Assuming that the errors estimated for SRTM (7–8%) and O_3 (3%) are independent, a total uncertainty of 13% is evaluated.

5 Conclusions

In this work we have shown that mean $j(NO_2)$ photolysis frequencies for the atmosphere simulation chamber SAPHIR can be predicted with high accuracy and precision using the SRTM approach described by Bohn and Zilken (2005). The remaining differences can be attributed to deficiencies of the model approach and technical problems concerning the condition of the chamber walls. With respect to the actinometric reference measurements, we estimate an accuracy of 7–8% for the $j(NO_2)$ based on SRTM, independent of external conditions. No change of $h^c_{jNO_2}$ was found within a period of one year and regular checks will be made to assure the long-term reliability of the measurements. Taking into account possible systematic errors of the actinometric $j(NO_2)$, photolysis frequencies within SAPHIR are accurate within 13%.

In future work the SRTM model and the radiometric input data could be improved as indicated by Bohn and Zilken (2005). Moreover, an actinometric determination of $j(O^1D)$ photolysis frequencies within SAPHIR will be developed to check the model predictions concerning wavelength dependence. Ozone measurements of higher precision and the enforcement of well mixed conditions would improve the precision and the accuracy of the actinometric $j(NO_2)$ measurements. Under these conditions, smaller systematic effects caused by deficient model assumptions could be investigated.

Acknowledgements. The authors thank A. Hofzumahaus for useful discussions. Financial support by the Helmholtz-Gemeinschaft (B. Bohn) is gratefully acknowledged.

Edited by: U. Pöschl

References

Atkinson, R., Baulch, D. L., Cox, R. A., Crowley, J. N., Hampson, R. F., Hynes, R. G., Jenkin, M. E., Rossi, M. J., and Troe, J.: Evaluated kinetic and photochemical data for atmospheric chemistry: Part 1 – gas phase reactions of O_x, HO_x, NO_x and SO_x species, Atmos. Chem. Phys., 4, 1461–1738, 2004, **SRef-ID: 1680-7324/acp/2004-4-1461**.

Bohn, B. and Zilken, H.: Model-aided radiometric determination of photolysis frequencies in a sunlit atmosphere simulation chamber, Atmos. Chem. Phys., 5, 191–206, 2005, **SRef-ID: 1680-7324/acp/2005-5-191**.

Brauers, T. and Rohrer, F.: Easy AtmoSpheric Chemistry: Manual Vers 2.9, available at http://www.fz-juelich.de/icg/icg-ii/easy_doc/, 1999.

Grant, R. H. and Heisler, G. M.: Obscured overcast sky radiance distributions for ultraviolet and photosynthetically active radiation, J. Appl. Meteorol., 36, 1336–1345, 1997.

Grant, R. H., Heisler, G. M., and Gao, W.: Clear sky radiance distributions in ultraviolet wavelength bands, Theo. Appl. Climatol., 56, 123–135, 1997.

Hofzumahaus, A., Kraus, A., and Müller, M.: Solar actinic flux spectroradiometry: A technique for measuring photolysis frequencies in the atmosphere, Appl. Opt., 38, 4443–4460, 1999.

Hofzumahaus, A., Lefer, B. L., Monks, P. S., Hall, S. R., Kylling, A., Mayer, B., Shetter, R. E., Junkermann, W., Bais, A., Calvert, J. G., Cantrell, C. A., Madronich, S., Edwards, G. D., Kraus, A., Müller, M., Bohn, B., Schmitt, R., Johnston, P., McKenzie, R., Frost, G. J., Griffioen, E., Krol, M., Martin, T., Pfister, G., Röth, E. P., Ruggaber, A., Swartz, W. H., Lloyd, S. A., and VanWeele, M.: Photolysis frequency of O_3 to $O(^1D)$: Measurement and modelling during the international photolysis frequency measurement and modelling intercomparision (IPMMI), J. Geophys. Res., 109, D8, D08S90, doi:10.1029/2003JD004333, 2004.

Kraus, A., Rohrer, F., and Hofzumahaus, A.: Intercomparison of NO_2 photolysis frequency measurements by actinic flux spectroradiometry and chemical actinometry during JCOM97, Geophys. Res. Lett., 27, 1115–1118, 2000.

Merienne, M. F., Jenouvrier, A., and Coquart, B.: The NO_2 absorption spectrum: 1. Absorption cross-sections at ambient temperature in the 300–500 nm region, J. Atmos. Chem., 20, 281–297, 1995.

Rohrer, F., Brüning, D., Grobler, E. S., Weber, M., Ehhalt, D. H., Neubert, R., Schüssler, W., and Levine, I.: Mixing Ratios and

photostationary state of NO and NO_2 observed during the POPCORN field campaign at a rural site in Germany, J. Atmos. Chem., 31, 119–137, 1998.

Rohrer, F., Bohn, B., Brauers, T., Brüning, D., Johnen, F.-J., Wahner, A., and Kleffmann, J.: Characterisation of the photolytic HONO source in the atmosphere simulation chamber SAPHIR, Atmos. Chem. Phys. Discuss., 4, 7881–7915, 2004, **SRef-ID: 1680-7375/acpd/2004-4-7881**.

Sander, S. P., Friedl, R. R., Ravishankara, A. R., Golden, D. M., Kolb, C. E., Kurylo, M. J., Huie, R. E., Orkin, V. L., Molina, M. J., Moortgat, G. K., and Finlayson-Pitts, B. J.: Chemical Kinetics and Photochemical Data for Use in Atmospheric Studies, Evaluation Number 14, JPL Publ. 02–25, 2003.

Shetter, R. E., Junkermann, W., Swartz, W. H., Frost, G. J., Crawford, J. H., Lefer, B. L., Barrick, J. D., Hall, S. R., Hofzumahaus, A., Bais, A., Calvert, J. G., Cantrell, C. A., Madronich, S., Müller, M., Kraus, A., Monks, P. S., Edwards, G. D., McKenzie, R., Johnston, P., Schmitt, R., Griffioen, E., Krol, M., Kylling, A., Dickerson, R. R., Lloyd, S. A., Martin, T., Gardiner, B., Mayer, B., Pfister, G., Röth, E. P., Koepke, P., Ruggaber, A., Schwander, H., and van Weele, M.: Photolysis frequency of NO_2: Measurement and modelling during the international photolysis frequency measurement and modelling intercomparision (IPMMI), J. Geophys. Res., 108, D16, 8544, doi:10.1029/2002JD002932, 2003.

Troe, J.: Are primary quantum yields of NO_2 photolysis at $\lambda \leq 398$ nm smaller than unity?, Z. Phys. Chem., 214, 573–581, 2000.

Volz-Thomas, A., Lerner, A., Pätz, H.-W., Schultz, M., McKenna, D. S., Schmitt, R., Madronich, S., and Röth, E.-P.: Airborne measurements of the photolysis frequency of NO_2, J. Geophys. Res., 101, D13, 18 613–18 627, 1996.